Surface-Enhanced Raman Spectroscopy for Facile DNA Detection using Gold Nanoparticle Aggregates Formed *via* Photoligation

Nguyen T. B. Thuy,[a] Ryoko Yokogawa,[a] Yoshinaga Yoshimura,[b] Kenzo Fujimoto,[a,b] Mikio Koyano[a] and Shinya Maenosono*[a]

Received (in XXX, XXX) Xth XXXXXXXXX 200X, Accepted Xth XXXXXXXXX 200X
First published on the web Xth XXXXXXXXX 200X
DOI: 10.1039/b000000x

We present a new type of nanoparticle-based DNA sensor using surface-enhanced Raman scattering (SERS) on gold nanoparticle (Au NP) aggregates formed by DNA photoligation. The DNA sensor exploits the photoligation reaction between oligodeoxynucleotides (ODNs) attached to the surfaces of Au NPs in the presence of target DNA (T-DNA). When hybridization takes place between the ODNs and T-DNA, Au NPs are covalently crosslinked to form aggregates *via* photoligation. Once the NP aggregates are formed, the interspace between Au NPs in the aggregate act as a stable "hot spot", and a SERS signal from the Raman-active molecules (sodium cacodylate) present in the hot spot is easily and sensitively detected. In contrast, a SERS signal is not detected if the hybridization is unsuccessful, because the stable hot spot does not form. This DNA sensor does not require an enzymatic reaction, fluorescent dye, precise temperature control, or complicated operating procedures.

Introduction

The development of highly sensitive, selective and inexpensive DNA detection methods is of great importance in the fields of medical research, clinical diagnosis,[1] forensic investigations and gene therapy because of the very low concentration of DNA in cells.[2-4] Up to now, many techniques have been proposed to improve the sensitivity, selectivity and reduce the cost of genetic diagnostics.[5-8] Conventional DNA detection methods involve the implementation of mass spectrometry[9] or gel electrophoresis.[10] However, these methods have some limitations because of relatively high cost and time-consuming operations. Other disadvantages such as photobleaching and overlapping peaks limit DNA detection systems based on optical methods using fluorescent dyes.[11] To overcome these problems, many researchers have proposed various other approaches for colorimetric detection of DNA hybridization based on the unique optical properties of gold nanoparticle (Au NP) aggregates.[12-17] For example, Mirkin and coworkers have developed a method for detecting polynucleotides that uses the distance-dependent optical properties of Au NPs modified with oligonucleotides.[2,12] Li and Rothberg showed that after the adsorption of single-stranded DNA on Au NPs, the NPs were stabilized against salt-induced aggregation.[18] This observation formed the basis for a colorimetric assay to identify specific DNA sequences. Recently, Storhoff *et al.* have developed a "spot-and-read" colorimetric detection method for identifying DNA which is also based on the distance-dependent optical properties of Au NPs with extraordinary sensitivity.[19] Unfortunately, these newly emerging techniques require carefully trained and skillful personnel as well as a relatively long analysis time. This is because their principles are based on the difference in the melting temperatures of the duplex formed between the allele-specific probe and the target DNA so they require stringent temperature control. Moreover, these techniques might have difficulty in distinguishing single-base imperfections that display a major difference in melting temperature. The limitations of these existing techniques would be inconvenient for practical clinical applications.[16]

Recently, various metal NP-based biosensors using localized surface plasmon resonance (LSPR) have been proposed,[20-24] and development of applications of LSPR has been a topical research subject.[25] The Au NP-based DNA sensors mentioned above are some noteworthy cases of LSPR biosensors. In particular, one of the most attractive extensions of LSPR sensors is their biosensing applications using surface-enhanced Raman scattering (SERS).[26-32] SERS is a surface sensitive phenomenon which results in the enhancement of Raman scattering by molecules absorbed on rough metal surfaces or metal colloid aggregates. The significant amplification of Raman scattering intensity is because of the electric field enhancement that occurs in the vicinity of small, interacting metal NPs that are illuminated with light resonance or near resonance with the LSPR frequency. SERS has attracted great interest in recent years as a powerful analytical tool that yields enormous structural information about the analyte, as well as quantitative information.[33] SERS-based sensors are highly sensitive, and thus, can be exploited in biosensing applications and have been successfully applied to analyze biologically relevant molecules, such as DNA,[34-38] proteins[39] and cells,[40] with high sensitivity and selectivity. However, the development of robust and reproducible SERS-enhancing substrates has long been a central task in SERS research.

To that end, we propose a unique and easy-to-operate NP-based SERS sensor for the detection of DNA sequences. The proposed DNA sensor exploits the photoligation reaction[41,42]

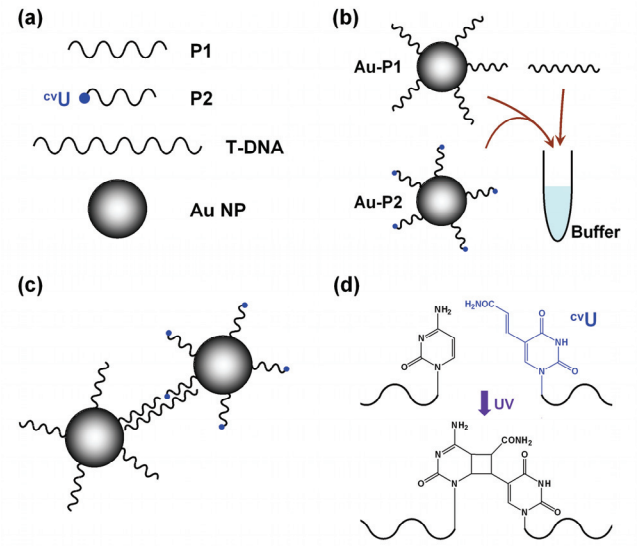

Fig. 1 Illustration of the DNA sensor. (a) Main components of the system. (b) Procedure to hybridize Au-P1, Au-P2, and T-DNA in cacodylate buffer. (c) Schematic depiction of the hybridized structure containing Au-P1, Au-P2, and T-DNA. (d) Chemical structures of the cytosine base at the 3'-end of P1 and ^{cv}U at the 5'-end of P2 before and after photoligation.

between oligodeoxynucleotides (ODNs) attached on the surfaces of Au NPs in the presence of target DNA (T-DNA). In this technique, two kinds of ODNs, a common probe (P1) and a specific discriminating probe (P2), are separately conjugated on the surface of Au NPs. These ODN-conjugated Au NPs are denoted as Au-P1 and Au-P2, respectively. When hybridization takes place between Au-P1 and T-DNA and between Au-P2 and T-DNA, the Au NPs covalently crosslink to form aggregates *via* photoligation between P1 and P2 as shown in Figure 1. Once the NP aggregates have formed, the interspace between Au NPs in the aggregate act as a stable "hot spot", and a SERS signal from the Raman-active molecules present in the hot spot is easily detected. In contrast, a SERS signal is not detected if the hybridization is unsuccessful, because a stable hot spot is not formed. The DNA sensor proposed here is simple, easy-to-use, rapid and robust, requiring no enzymatic reaction, fluorescent dye, precise temperature control, or complicated operating conditions.

Experimental

Materials

Trisodium citrate hydrate (cat. no 194-13245), 3-aminopropyltrimethoxysilane (cat. no 323-74-352), calcium chloride ($CaCl_2$, purity 95 %), and sodium chloride (NaCl, purity 99.5 %) were purchased from Wako Pure Chemical Industries, Ltd., Japan. Gold(III) chloride trihydrate ($HAuCl_4.3H_2O$, cat. no. 1525-26) was purchased from MP Biomedicals, LLC, France. Methanol, acetone, and sulfuric acid were purchased from Kanto Chemical Co., Inc., Japan. Cacodylate buffer solution (0.2 M, cat. no 37237-35) was purchased from Nacalai Tesque, Inc., Japan. For ODN synthesis, thiol-modifier C6 S-S, and 3'-thiol-modifier C3 S-S CGP, the reagents for the DNA synthesizer such as A, G, C, T-β-cyanoethyl phosphoramidite, and CPG support were purchased from Glen Research, USA. Calf intestine alkaline phosphatase was purchased from Promega, Japan. Nucleate 5'-nucleotidohydrolase (3'-phosphohydrolase) (Nuclease P1) was purchased from Yamasa Corp., Japan.

Equipment

UV-visible spectroscopy

UV-visible absorption spectra of the Au NP dispersions were obtained using a Beckman Coulter DU800 UV/VIS spectrometer. The spectra were collected over the range of 200-800 nm.

Dynamic light scattering (DLS) and zeta potential (ZP) measurements

DLS and ZP measurements were performed on diluted Au NP dispersions at room temperature using a Zetasizer Nano ZS ZEN 3600 (Malvern, UK).

Raman spectroscopy

Raman spectra were obtained with a Kr^+ ion laser (wavelength 647.1 nm, power 100 mW), using a Horiba-Jobin Yvon Ramanor T64000 triple monochromator equipped with a CCD detector. The non-polarized Raman scattering measurements were set under a microscope sample holder using a 180° backscattering geometry at room temperature. The laser spot diameter was 1 μm. As an acquisition time was 30 sec per spectrum, we averaged three spectra taken from same area.

Transmission electron microscopy (TEM)

TEM measurements were performed to determine the average diameter and the morphology of Au NPs and their aggregates using a Hitachi 7100 transmission electron microscope operated at 100 kV. TEM samples were prepared by dropping 5 μL of the Au NP dispersions onto carbon-coated copper grids under ambient conditions and allowing them to evaporate slowly at room temperature.

UV irradiation for photoligation

Photoligation between the cytosine base at the 3'-end of P1 and 5-carboxylvinyl-2'-deoxyuridine at the 5'-end of P2 was performed using an UV-LED (Omron, ZUV, wavelength 366±15 nm, power 1600 mW/cm^2) at a distance of 1.5 cm at 0 °C for 15 min.

ODN synthesis

ODN sequences 5'- HS-ACTCACAGTTTTCAC -3' (15-mer, 5'-SH, P1), 5'-^{cv}UTCAGTGTA-SH -3' (9-mer, 3'-SH, P2), and 5'-TACACTGAAGTGAAAACTGTGAGTG -3' (25-mer, T-DNA) were synthesized by the conventional phosphoramidite method using an Applied Biosystems 3400 DNA synthesizer. Here ^{cv}U denotes a 5-carboxylvinyl-2'-deoxyuridine moiety that acts as a photolinking group. The coupling efficiency was determined using a trityl monitor. The coupling efficiency and coupling time of the crude mixture of the phosphoramidite were 97 % and 999 s, respectively. The coupled mixtures were deprotected by incubation with 28 % ammonia for 8 h at 55 °C and were purified on a Chemcobond 5-ODS-H column (10×150 mm) by reversed-phase high

performance liquid chromatography (HPLC); 0.05 M ammonium formate containing 3-20 % CH_3CN was used as the eluent with a linear gradient (30 min) at a flow rate of 3.0 mL/min. ODNs were fully digested with calf intestine alkaline phosphatase (50 U mL^{-1}) and Nuclease P1 (50 U mL^{-1}) at 37 °C for 4 h. The digested samples were analyzed using HPLC (Supplementary Information Figures S1-S3). The concentration of each ODN was determined by comparing the peak areas with standard solutions that contained dA, dG, dC, and dT at a concentration of 0.1 mM. Preparation of ODNs was confirmed by MALDI-TOF-MS analysis (Supplementary Information Figures S4-S6).

Au NP synthesis

Au NPs with average diameter of 15 nm (standard deviation ≤15 %) were synthesized by the citrate thermal reduction method.[43] The LSPR extinction peak was located at 520 nm. The citrate ions were used as a reducing agent, as well as a protective capping agent to stabilize the Au NPs in the medium. Typically, Au NPs were synthesized in a 100 mL round-bottom three-neck flask equipped with a thermo-couple. An aqueous solution of $HAuCl_4.3H_2O$ (50 mL, 1 mM) was stirred vigorously and heated to reflux at 100 °C. Then, aqueous trisodium citrate (5 mL, 38.8 mM) was rapidly injected in the flask. After the injection of sodium citrate, the color of reaction mixture changed from yellow to burgundy indicating the formation of Au NPs, the mixture was stirred for 15 min at 100 °C. The mixture was cooled to room temperature and then filtered using a 0.45 μm syringe filter (Sartorius Stedim Biotech GmbH, Germany). The concentration of Au NPs was estimated to be 10.4 nM using the extinction coefficient of 15 nm Au NPs of $\varepsilon_{520} \cong 2.40 \times 10^8$ M^{-1} cm^{-1}.[44]

Preparation of substrates

Glass substrates were used after surface modification. The surface modification was conducted according to the procedure reported by Watts *et al.*[45] Glass slides (Matsunami micro slide glass, 2.6×7.6 cm^2) were cleaned by sonication in acetone for 10 min, followed by 10 min ultrasonic cleaning in methanol. After drying for 20 min at 100 °C in air, the slides were immersed in concentrated sulfuric acid for 2 h. The slides were rinsed thoroughly with distilled water 6 times and then dried for 20 min at 100 °C in air. Surface modification of the glass substrates was performed by soaking the substrates in a mixture of 3-aminopropyltrimethoxysilan (APTMS, 3 mL) in methanol (60 mL) for 4 h at room temperature. After soaking, the glass substrates were washed thoroughly using a copious amount of methanol to remove the excess APTMS. The substrates were stored in methanol at room temperature when not in use. The substrates were dried for 20 min at 100 °C in air immediately prior to use. APTMS modification of the glass slides was confirmed by measuring the water contact angle.

Preparation of Au-P1 and Au-P2

The citrate capped Au NPs were modified with thiolated ODNs (P1 or P2) through a simple protocol. An aqueous solution of $CaCl_2$ (50 μL, 10 mM) was added to an aqueous dispersion of the Au NPs (1 mL, 10.4 nM). Subsequently, 50 μL of the NP dispersion was divided and mixed with an aqueous solution of ODN (P1 or P2, 50 μL, 100 μM) to conjugate thiolated ODNs on the surfaces of the Au NPs. After mixing, the dispersion was incubated at 40 °C for 5 h in the dark. Note that the ODN containing ^{cy}U is light sensitive, and thus, should be protected from exposure to UV radiation. ODN-modified Au NPs (Au-P1 and Au-P2) were stored at 4 °C in the dark until just prior to use.

Hybridization and photoligation

2 μL of each dispersion containing Au-P1 or Au-P2 was taken from their respective neat dispersions. Then, both the Au-P1 and Au-P2 dispersions were mixed with 2 μL of T-DNA solution (100 μM) in a cacodylate (50 mM)/NaCl (100 mM) buffer at room temperature in the dark. The final composition of the mixture (total volume 10 μL) was as follows: T-DNA 20 μM; sodium cacodylate [$(CH_3)_2AsOONa$] 50 μM; NaCl 100 μM. Subsequently, the mixture was cooled down to 0 °C and irradiated with UV light with a wavelength of 366±15 nm for 15 min to promote photoligation. The mixture was then heated at 90 °C for 3 min using a Thermal Cycler MP TP-3000 (Takara, Japan) to denature the DNA. Then, 2 μL of the dispersion was dropped on the APTMS-modified glass substrate and dried at 90 °C for 5 min.

Results and discussion

Preparation of ODN-modified Au NPs

The as-synthesized Au NPs are capped with citrate ions so the surfaces of the NPs are negatively charged. The ODNs are also negatively charged. Hence, the conjugation reaction of thiolated ODNs to Au NPs was unsuccessful when one simply mixed the Au NPs and ODNs because of the electrostatic repulsion between the Au NPs and ODNs. Therefore, Ca^{2+} ions were added to the NP dispersion to screen the negative charge of both species. Ca^{2+} ions were chosen to reduce the electrostatic repulsion between the Au NPs and ODNs because $CaCl_2$ solution is routinely used to enhance the efficiency of the genetic transformation of *E. coli* with plasmid DNA. It is well known that divalent cations, such as Ca^{2+}, make the cell membrane permeable to plasmid DNA, effectively reducing the electrostatic repulsion between DNA and cell membrane. However, if the concentration of Ca^{2+} ions was too high, the Au NPs aggregated before the ODNs were attached on the NP surfaces. Thus, the concentration of Ca^{2+} screening the charges of NPs and ODNs was carefully controlled to avoid aggregation of the Au NPs.

Figure 2 shows UV-vis absorption spectra of the Au NP dispersions taken immediately after adding different volumes of $CaCl_2$ solution (10 mM). The volume of the Au NP dispersion prior to adding the $CaCl_2$ solution is 1 mL. When the volume of $CaCl_2$ solution added was larger than 100 μL,

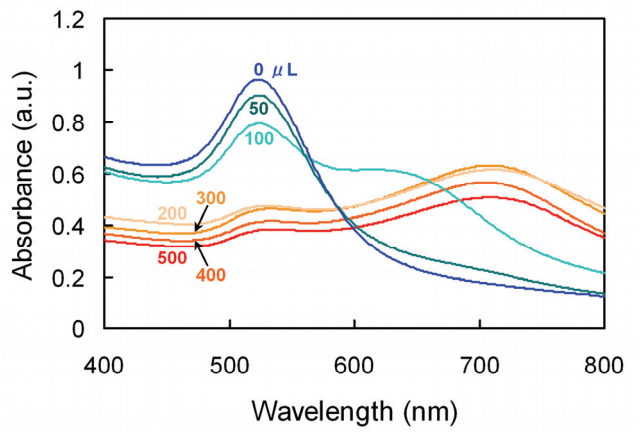

Fig. 2 Absorption spectra of the Au NP dispersions containing different volumes of $CaCl_2$ solution. From top to bottom: 0, 50, 100, 200, 300, 400, and 500 μL of $CaCl_2$ solution added to 1 mL of Au NP dispersion, respectively.

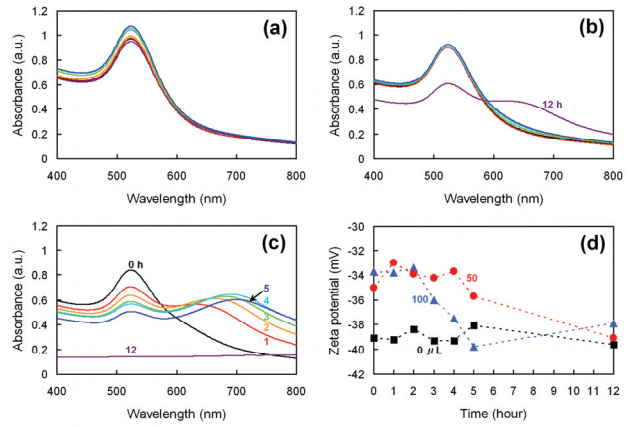

Fig. 3 Time dependence of absorption spectra of the Au NP dispersions containing (a) 0, (b) 50 and (c) 100 μL of $CaCl_2$ solution. Black, red, orange, green, light blue, blue, and purple lines represent 0, 1, 2, 3, 4, 5, and 12 h incubation periods, respectively. (d) Time dependence of the ZP of Au NP dispersions containing 0 (black), 50 (red) and 100 μL (blue) of $CaCl_2$ solution.

the extended plasmon band (EPB) was clearly seen between 600 and 800 nm, indicating the formation of Au NP aggregates. A negligible change in the absorption spectrum was observed when the volume of $CaCl_2$ solution added was 50 μL, signifying that the Au NPs were still well dispersed during the experimental time range. Subsequently, the aggregation rate (stability) of the Au NPs with the addition of 0, 50 and 100 μL of $CaCl_2$ solution was investigated. Because the ODNs do not conjugate to the Au NPs after aggregation, the incubation was stopped before significant aggregation took place. Figures 3a, 3b and 3c show the variation of the absorption spectra of the Au NP dispersions over time with the addition of 0, 50 and 100 μL of $CaCl_2$ solution, respectively. As seen in Figure 3a, the Au NP dispersion with no added $CaCl_2$ is remarkably stable over the experimental time range (12 h). In the case of the Au NP dispersion with 50 μL of $CaCl_2$ solution added (Figure 3b), no sign of aggregation was observed up to 5 h after the addition of the $CaCl_2$ solution. However, after 12 h incubation, the EPB was clearly seen in the absorption spectrum. In the case of the Au NP dispersion containing 100 μL of $CaCl_2$ solution (Figure 3c), the EPB was clearly observed within 1 h of the addition of the $CaCl_2$ solution.

To confirm the screening effect of the Ca^{2+} ions, the zeta potential (ZP) of the Au NPs was measured for each dispersion containing different Ca^{2+} concentrations (Figure 3d). The ZP of the as-synthesized Au NPs was constant at about −39 mV. After addition of the $CaCl_2$ solution, ZP decreased to about −34 mV regardless of the volume of $CaCl_2$ solution added. However, in the case of the Au NP dispersion containing 100 μL of $CaCl_2$ solution, ZP quickly returned to the value of the as-synthesized Au NPs. This can be explained by the ZP measurement technical mechanism. ZP was estimated by measuring the mobility of particles using laser Doppler anemometry under an alternating electric field. Therefore, when the aggregates precipitate in the capillary cell, their ZP cannot be measured, so only the ZP of the remaining mobile (non-aggregated) NPs is detected. The non-aggregated NPs would have almost the same ZP value as the as-synthesized Au NPs, so aggregation caused the ZP to return to the value of as-synthesized Au NPs. On the other hand, for the Au NP dispersion containing 50 μL of $CaCl_2$ solution, ZP remained constant at around −34 mV for the first 5 h, and then returned to the value of the as-synthesized Au NPs. These results are consistent with those of the UV-vis spectroscopy. In consequence, the conjugation reaction of thiolated ODNs to Au NPs was performed for 5 h after the addition of 50 μL of $CaCl_2$ solution (10 mM). The slight decrease in the ZP is thought to be enough to enhance the conjugation reaction rate, while preventing aggregation of the NPs.

To confirm the conjugation of thiolated ODNs on the surfaces of the Au NPs, Raman measurements were performed. The ODN sequence used was 5'-ACGCAGGCAC-SH -3' (10-mer, 3'-SH), and the Raman spectrum was obtained immediately after dropping 2 μL of the dispersion (Au NPs/ODNs/$CaCl_2$ mixture) on an APTMS-modified glass substrate. Figure 4a shows the Raman spectra of samples prepared with different incubation times. Several Raman peaks start to appear after a 2 h incubation period. The 610 cm^{-1} band is assigned to the ring breathing mode of guanine, which is sensitive to the conformation, and the 780 cm^{-1} band is assigned to the ring breathing mode of cytosine.[46] In Figure 4b, the temporal variations of the 610 cm^{-1} and the 780 cm^{-1} band intensities were plotted. The peak intensities increased with incubation time and were almost saturated after a 3 h incubation period, suggesting that the conjugation reaction of ODNs on the Au NP surfaces was complete. That is, the number of ODN molecules present in the hot spot increases, because the ODNs were successfully immobilized on the Au NP surfaces. Considering the results shown in Figs. 3 and 4, the optimum incubation time for the conjugation reaction of ODNs on the Au NP surfaces was determined to be 5 h.

After conjugation, the ODN-modified Au NPs exhibited almost identical UV-vis spectra. A negligible shift in the

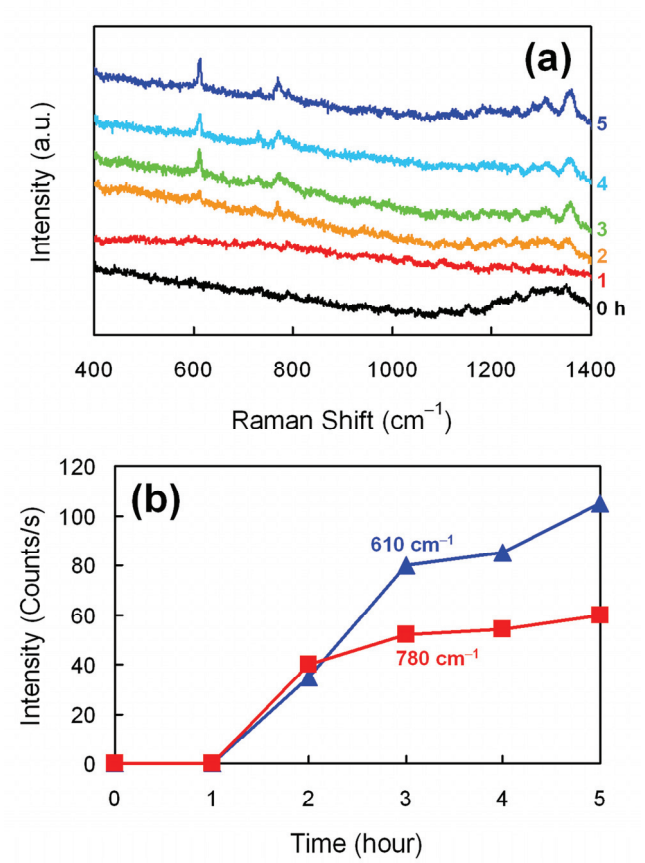

Fig. 4 (a) Raman spectra of Au NPs incubated with ODNs for different periods at 40 °C. Black, red, orange, green, light blue, and blue lines represent 0, 1, 2, 3, 4, and 5 h incubation periods, respectively. (b) Temporal variations of the 610 cm^{-1} (blue triangles) and the 780 cm^{-1} (red squares) band intensities.

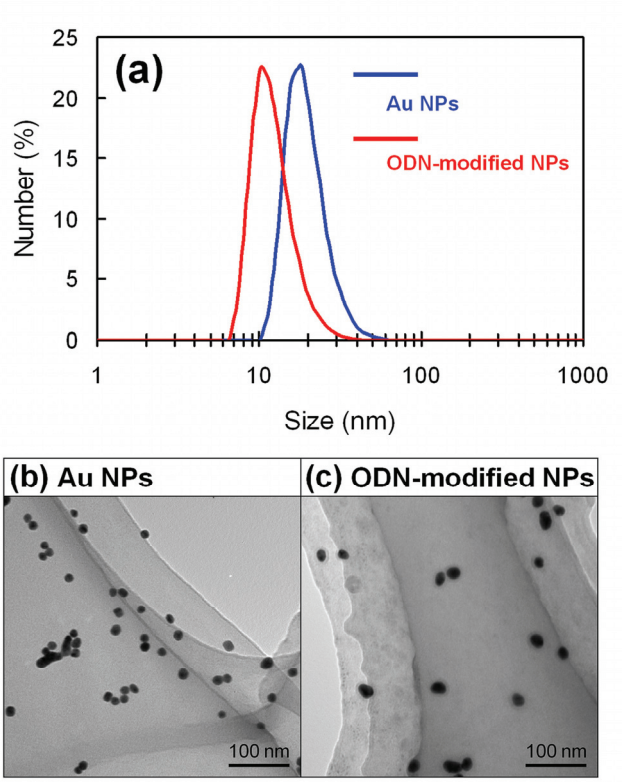

Fig. 5 (a) Size distributions of as-synthesized (blue curve) and ODN-modified (red curve) Au NPs dispersed in water measured by DLS, and TEM images of (b) as-synthesized and (c) ODN-modified Au NPs.

LSPR band from 520 nm to 522 nm was observed between the as-synthesized and ODN-modified Au NPs (data not shown). This suggests that Au NPs were stabilized better against Ca^{2+} with ODNs conjugated on their surfaces, because the UV-vis spectrum of bare Au NPs after the addition of 50 μL of $CaCl_2$ solution (Fig. 3b) was not completely identical to that of as-synthesized Au NPs (Fig. 3a). Figure 5a shows the size distributions of as-synthesized and ODN-modified Au NPs dispersed in water, measured by dynamic light scattering (DLS). Interestingly, the ODN-modified NPs were smaller on average than the unmodified Au NPs. This result implies that the repulsion force between ODN-modified NPs is larger than that of the unmodified, citrate-capped NPs because the higher electrostatic and steric repulsion potentials of ODNs, compared with those of the citrate ions, suppress the clustering of Au NPs. Figures 5b and 5c show TEM images of the as-synthesized and ODN-modified NPs, respectively. The ODN-modified NPs show larger separation from each other than the unmodified NPs, which is consistent with the size distributions of the two types of Au NP.

DNA hybridization detection using SERS spectroscopy

Most examples of SERS-based biosensors use a Raman-active dye as a reporter molecule to obtain a strong SERS signal,[47] because the SERS signal from the biorelevant molecule itself is usually weak. In general, the system becomes more complicated and more difficult to operate as the number of components increases. Therefore, in our DNA detection system, sodium cacodylate is used as a reporter molecule as well as a hybridization buffer. The 608 cm^{-1} vibration of cacodylate (symmetric AsO_2 stretch) was the intensity standard used by Blazej and Peticolas in their pioneering studies of Raman excitation profiles of nucleic acid bases.[48] The Raman scattering cross section of the 608 cm^{-1} vibration of cacodylate at 647 nm was determined to be 40±4 μbarns where a barn is 10^{-24} cm^2.[49] Figure 6a shows the Raman spectra of sodium cacodylate obtained in liquid (solution) and solid (crystal) phases. The cacodylate vibrations are visible as a pair of bands centered at 605 cm^{-1} and 639 cm^{-1} (AsO_2 stretch) in the liquid phase sample. In the solid phase, the higher energy peak shifted toward 600 cm^{-1}, while the lower energy peak disappeared.

Figure 6b shows the dependence of the UV irradiation time on the Raman spectrum of cacodylate in the sample deposited on the APTMS-modified glass substrate. The AsO_2 stretching vibrations are clearly observed as a pair of bands centered at 608 cm^{-1} and 638 cm^{-1} in both samples irradiated with UV light for 15 and 30 min. The inset in Figure 6b shows the intensity of the 608 cm^{-1} peak versus UV irradiation time. The Raman spectra were taken at ten different positions for each sample. Consequently, it exemplifies that the intensity of the

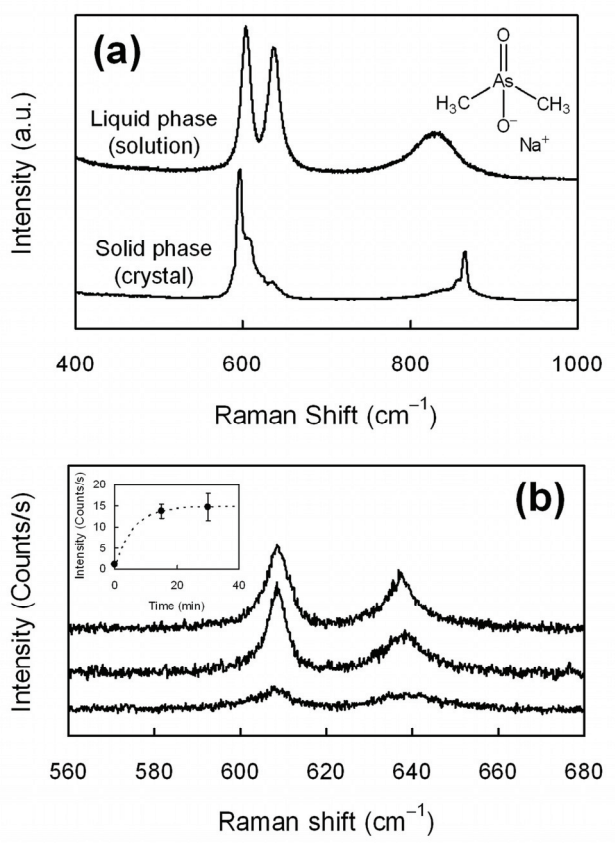

Fig. 6 (a) Raman spectra of sodium cacodylate obtained in liquid (top) and solid (bottom) phases. The inset shows the chemical structure of sodium cacodylate. (b) Changes in the Raman spectrum of cacodylate in the sample deposited on the APTMS-modified glass substrate plotted versus UV irradiation time (0, 15, and 30 min from bottom to top). The inset shows the intensity of the peak at 608 cm^{-1} versus UV irradiation time.

608 cm^{-1} band of the samples irradiated by UV is notably higher than that of the sample not exposed to UV irradiation. Additionally, the intensity of the 608 cm^{-1} band did not change when the UV irradiation time was prolonged from 15 min to 30 min. These results imply that Au-P1 and Au-P2 are successfully linked *via* photoligation in the presence of T-DNA, and thus, the SERS signal of cacodylate present in the hot spot can be obtained. Moreover, 15-min of UV irradiation seems to be long enough to allow completion of the photoligation reaction. Hence, the UV irradiation time was fixed at 15 min.

To confirm that the increased intensity of the 608 cm^{-1} band was caused by photoligation of Au-P1 and Au-P2, we carried out control experiments using Raman measurements of samples lacking UV exposure, T-DNA, Au-P1 and Au-P2, deposited on the APTMS-modified glass substrate. Figures 7a, 7b, 7c, 7d, and 7e show the Raman spectra of the complete (containing Au-P1, Au-P2, T-DNA, and exposed to UV irradiation), and the samples lacking UV exposure, T-DNA, Au-P1, and Au-P2, respectively. The Raman spectra taken at eight different positions for each sample were plotted in each figure. As seen in Figs. 7b-e, the intensities of the band at 608 cm^{-1} of the control samples are statistically the same, and are evidently much lower than that of the complete sample (Fig. 7a). This result clearly indicates that the complete set of conditions (Au-P1, Au-P2, T-DNA, and UV irradiation) is necessary to obtain the SERS signal from cacodylate, that is, the hybridization detection scheme shown in Figure 1 is realized in our experiments. It is noteworthy that we were able to reproduce our experimental results at least three times and always obtained the same results, indicating this system is robust and highly reproducible. As can be seen in Figure 7a, however, the intensity of the 608 cm^{-1} peak varied considerably within the same sample. This is due to the microscopic inhomogeneity of the sample, i.e., the probability of finding Au NP aggregates (hot spots) within the laser beam differs according to the location in the sample, because the concentration of Au NPs is quite low. Figure 7f shows the histogram of the intensity of the 608 cm^{-1} peak. Amplified signals with an intensity of greater than 10 counts/s are observed only in the complete sample, and can be attributed to SERS signals from aggregates formed *via* photoligation. On the other hand, all of the samples have weak signals with an intensity of less than 4 counts/s, which are the signals from positions without a hot spot, and can be regarded as the background. The signals with an intensity ranging from 4 to 10 counts/s observed in the perfect, Au-P1-less and Au-P2-less samples may arise from hot spots formed *via* natural aggregation during drying. To reduce the variation in the intensity of the SERS and increase the signal-to-noise ratio, the samples must be homogeneous. However, if a monolayer (or multilayer) of Au NPs is formed on the substrate surface, the background intensity will increase significantly, as the density of naturally-formed hot spots will markedly increase because of decreases in the inter-particle separation distance. The processing of more uniform materials is part of our ongoing work.

To further confirm the formation of aggregates *via* crosslinking between Au-P1 and Au-P2 through hybridization with T-DNA followed by photoligation between P1 and P2, TEM images were taken of all of the samples (Figure 8). In Fig. 8, TEM images taken at two different arbitrarily selected positions in the same sample are shown for all of the samples. Obviously, large aggregates are observed only in the perfect sample (Fig. 8a), while only single, isolated NPs or small clusters of NPs are seen in the imperfect samples (Fig. 8b-e). The TEM images shown in Fig. 8b-e are quite similar to Fig. 5c. The mean surface-to-surface separation distance between the NPs in Fig. 8a is estimated to be 3.2 nm, which is a significantly larger value than that of citrate-capped Au NPs (1.4 nm), supporting the formation of the Au-P1-P2-Au bond. However, 3.2 nm is only approximately one third of the total length of P1 (6.3 nm) and P2 (3.8 nm), and thus, the Au-P1-P2-Au bond is thought to be bent in the interspaces between Au NPs.

Conclusions

We present a simple and easy-to-use DNA sensor obtained by measuring the surface-enhanced Raman scattering (SERS) of crosslinked Au NP aggregates. The DNA sensor uses

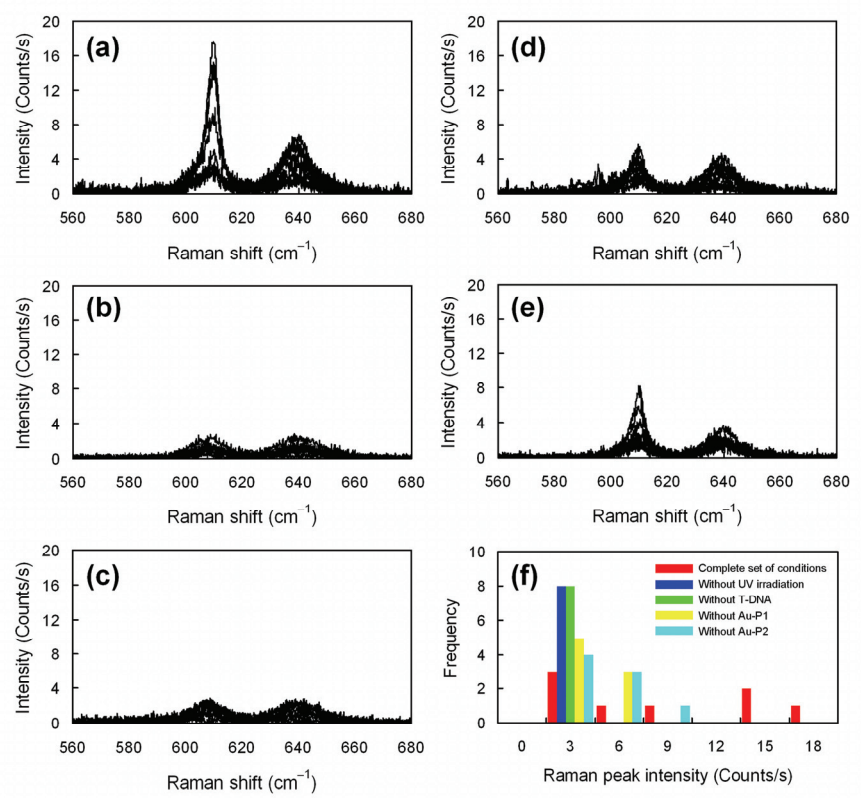

Fig. 7 Raman spectra of (a) perfect (Au-P1+Au-P2+T-DNA+UV), (b) UV-less (Au-P1+Au-P2+T-DNA), (c) T-DNA-less (Au-P1+Au-P2+UV), (d) Au-P1-less (Au-P2+T-DNA+UV), and (e) Au-P2-less (Au-P1+T-DNA+UV) samples. (f) Histogram of the intensity of the 608 cm^{-1} peak. Red, blue, green, yellow, and light blue bars correspond to the perfect, UV-less, T-DNA-less, Au-P1-less, and Au-P2-less samples, respectively.

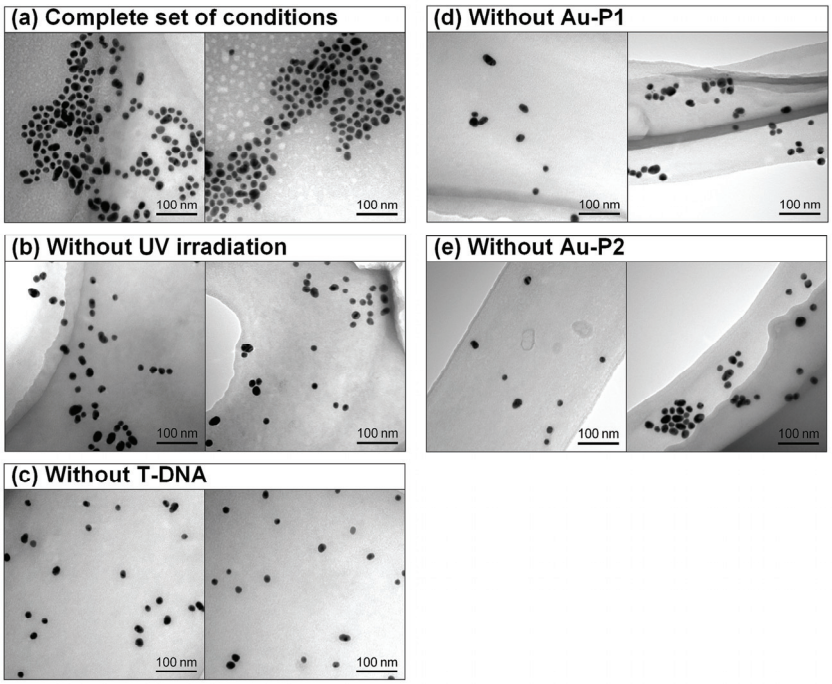

Fig. 8 TEM images of the samples: (a) perfect, (b) UV-less, (c) T-DNA-less, (d) Au-P1-less, and (e) Au-P2-less.

photoligation to achieve DNA recognition without requiring an enzymatic reaction, fluorescent dye, precise temperature control, or complicated operating conditions. The sensor operates well with a minute amount of target DNA (T-DNA) (~20 pmol), making it extremely sensitive. Au NPs conjugated with a common probe (Au-P1) and a specific discriminating probe with a photo-linking group at the 5' end (Au-P2) were simultaneously hybridized with T-DNA. Then, Au-P1 and Au-P2 were covalently linked to form a Au-P1-P2-Au bond by UV irradiation. The SERS signal of cacodylate ions, which act as reporter molecules, present in the interspaces between Au NPs was successfully detected. The incomplete set of conditions, lacking components such as Au-P1, Au-P2, T-DNA, or UV exposure, did not clearly produce the SERS signal. The results explicitly indicate that our sensor is feasible. However, in this study, we only used fully matched sequences, i.e., there was no mismatch between P1 and T-DNA, and between P2 and T-DNA. The match/mismatch discrimination performance of the DNA sensor is part of our ongoing work on this research topic.

DNA photoligation can be used for the potential application as a tool for molecular biology research such as the specific detection of DNA or RNA molecules. We anticipate that this new concept of DNA sensor using SERS on Au NP aggregates formed by DNA photoligation will be the starting point for the development of a practical assay for the quantification of a multitude of DNA and noncoding RNA in living cells.

Acknowledgements

The authors would like to thank the Vietnamese Government for a 322 scholarship. Dr. Ha Minh Hiep (Osaka University) is thanked for his valuable comments. We thank Dr. Derrick Mott for his careful reading of, and useful comments about, the manuscript.

Notes and references

[a] *School of Materials Science, Japan Advanced Institute of Science and Technology, 1-1 Asahidai, Nomi, Ishikawa 923-1292, Japan. Fax: +81 761 51 1625; Tel: +81 761 51 1611; E-mail: shinya@jaist.ac.jp*

[b] *Innovation Plaza Ishikawa, Japan Science and Technology Agency, 1-1 Asahidai, Nomi, Ishikawa 923-1292, Japan.*

† Electronic Supplementary Information (ESI) available: Results of HPLC and MALDI-TOF MS analyses of the ODNs. See DOI: 10.1039/b000000x/

1. S. Razin, *Mol. Cell. Probes*, 1994, **8**, 497-511.
2. R. Elghanian, J. J. Storhoff, R. C. Mucic, R. L. Letsinger and C. A. Mirkin, *Science*, 1997, **277**, 1078-1081.
3. K. Sato, K. Hosokawa and M. Maeda, *J. Am. Chem. Soc.*, 2003, **125**, 8102-8103.
4. W. Lian, S. A. Litherland, H. Badrane, W. Tan, D. Wu, H. V. Baker, P. A. Gulig, D. V. Lim and S. Jin, *Anal. Biochem.*, 2004, **334**, 135-144.
5. D. J. Lockhart and E. A. Winzeler, *Nature*, 2000, **405**, 827-836.
6. C. M. Niemeyer, *Angew. Chem. Int. Ed.*, 2001, **40**, 4128-4158.
7. B. W. Kirk, M. Feinsod, R. Favis, R. M. Kliman and F. Barany, *Nucleic Acids Res.*, 2002, **30**, 3295-3311.
8. C. H. Liu, Z. P. Li, B.-A. Du, X. R. Duan and Y. C. Wang, *Anal. Chem.*, 2006, **78**, 3738-3744.
9. P. Ross, L. Hall, I. Smirnov and L. Haff, *Nat. Biotechnol.*, 1998, **16**, 1347-1351.
10. D. Schmalzing, A. Belenky, M. A. Novotny, L. Koutny, O. Salas-Solano, S. El-Difrawy, A. Aram, P. Matsudaira and D. Ehrlich, *Nucleic Acids Res.*, 2000, **28**, e43.
11. X. Fang, X. Liu, S. Schuster and W. Tan, *J. Am. Chem. Soc.*, 1999, **121**, 2921-2922.
12. C. A. Mirkin, R. L. Letsinger, R. C. Mucic and J. J. Storhoff, *Nature*, 1996, **382**, 607-609.
13. J. J. Storhoff, R. Elghanian, R. C. Mucic, C. A. Mirkin and R. L. Letsinger, *J. Am. Chem. Soc.*, 1998, **120**, 1959-1964.
14. Y. P. Bao, M. Huber, T. F. Wei, S. S. Marla, J. J. Storhoff, U. R. Müller, *Nucleic Acids Res.*, 2005, **33**, e15.
15. J. Liu and Y. Lu, *J. Am. Chem. Soc.*, 2005, **127**, 12677-12683.
16. J. Li, X. Chu, Y. Liu, J. H. Jiang, Z. He, Z. Zhang, G. Shen and R. Q. Yu, *Nucleic Acids Res.*, 2005, **33**, e168.
17. K. Cho, Y. Lee, C. H. Lee, K. Lee, Y. Kim, H. Choi, P. D. Ryu, S.Y. Lee and S. W. Joo, *J. Phys. Chem. C*, 2008, **112**, 8629-8633.
18. H. X. Li and L. J. Rothberg, *J. Am. Chem. Soc.*, 2004, **126**, 10958-10961.
19. J. J. Storhoff, A. D. Lucas, V. Garimella, Y. P. Bao and U. R. Müller, *Nat. Biotechnol.*, 2004, **22**, 883-887.
20. M. D. Malinsky, K. L. Kelly, G. C. Schatz and R. P. Van Duyne, *J. Am. Chem. Soc.*, 2001, **123**, 1471-1482.
21. A. J. Haes and R. P. Van Duyne, *J. Am. Chem. Soc.*, 2002, **124**, 10596-10604.
22. J. C. Riboh, A. J. Haes, A. D. McFarland, C. R. Yonzon and R. P. Van Duyne, *J. Phys. Chem. B*, 2003, **107**, 1772-1780.
23. A. D. McFarland and R. P. Van Duyne, *Nano Lett.*, 2003, **3**, 1057-1062.
24. T. Endo, S. Yamamura, N. Nagatani, Y. Morita, Y. Takamura and E. Tamiya, *Sci. Technol. Adv. Mater.*, 2005, **6**, 491-500.
25. K. A. Willets and R. P. Van Duyne, *Annu. Rev. Phys. Chem.*, 2007, **58**, 267-297.
26. S. Nie and S. R. Emory, *Science*, 1997, **275**, 1102-1106.
27. K. Kneipp, Y. Wang, H. Kneipp, L. T. Perelman, I. Itzkan, R. R. Dasari and M. S. Feld, *Phys. Rev. Lett.*, 1997, **78**, 1667-1670.
28. A. Campion and P. Kambhampati, *Chem. Soc. Rev.*, 1998, **27**, 241-250.
29. M. Moskovits, *J. Raman Spectrosc.*, 2005, **36**, 485-496.
30. G. A. Baker and D. S. Moore, *Anal. Bioanal. Chem.*, 2005, **382**, 1751-1770.
31. T. Vo-Dinh, F. Yan and M. B. Wabuyele, *J. Raman Spectrosc.*, 2005, **36**, 640-647.
32. J. Kneipp, H. Kneipp, W. L. Rice and K. Kneipp, *Anal. Chem.*, 2005, **77**, 2381-2385.
33. R. Stosch, A. Henrion, D. Schiel and B. Guttler, *Anal. Chem.*, 2005, **77**, 7386-7392.
34. T. Vo-Dinh, L. R. Allain and D. L. Stokes, *J. Raman Spectrosc.*, 2002, **33**, 511-516.
35. S. E. J. Bell and N. M. S. Sirimuthu, *J. Am. Chem. Soc.*, 2006, **128**, 15580-15581.
36. A. J. Bonham, G. Braun, I. Pavel, M. Moskovits and N. O. Reich, *J. Am. Chem. Soc.*, 2007, **129**, 14572-14573.
37. G. Braun, S. J. Lee, M. Dante, T. Q. Nguyen, M. Moskovits and N. Reich, *J. Am. Chem. Soc.*, 2007, **129**, 6378-6379.
38. D. G. Thompson, A. Enright, K. Faulds, W. E. Smith and D. Graham, *Anal. Chem.*, 2008, **80**, 2805-2810.
39. Y. Wang, H. Wei, B. Li, W. Ren, S. Guo, S. Dong and E. Wang, *Chem. Commun.*, 2007, 5220-5222.
40. K. Kneipp, A. S. Haka, H. Kneipp, K. Badizadegan, N. Yoshizawa, C. Boone, K. E. Shafer-Peltier, J. T. Motz, R. R. Dasari and M. S. Feld, *Appl. Spectrosc.*, 2002, **56**, 150-154.
41. K. Fujimoto, S. Matsuda, N. Takahashi and I. Saito, *J. Am. Chem. Soc.*, 2000, **122**, 5646-5647.
42. S. Ogasawara, Y. Kyoi and K. Fujimoto, *ChemBioChem*, 2007, **8**, 1520-1525.
43. G. Frens, *Nat. Phys. Sci.*, 1973, **241**, 20-22.
44. J. J. Storhoff, A. A. Lazarides, C. A. Mirkin, R. L. Letsinger and G. C. Schatz, *J. Am. Chem. Soc.*, 2000, **122**, 4640-4650.

45. O. Seitz, M. M. Chehimi, E. Cabet-Deliry, S. Truong, N. Felidj, C. Perruchot, S. J. Greaves and J. F. Watts, *Colloid. Surf. A*, 2003, **218**, 225-239.
46. J. D. Gelder, K. D. Gussem, P. Vandenabeele and L. Moens, *J. Raman Spectrosc.*, 2007, **38**, 1133-1147.
47. X. Qian, X. Zhou and S. Nie, *J. Am. Chem. Soc.*, 2008, **130**, 14934-14935.
48. D. C. Blazej and W. L. Peticolas, *Proc. Natl. Acad. Sci.*, 1977, **74**, 2639-2643.
49. M. O. Trulson and R. A. Mathies, *J. Chem. Phys.*, 1986, **84**, 2068-2074.